AGU PUBLICATIONS

Geophysical Research Letters

RESEARCH LETTER
10.1002/2016GL068604

Key Points:
- First geodetic image of heterogeneous interseismic coupling on a continental LANF
- The locked portion of the Alto Tiberina LANF can potentially be the locus of $M > 6$ earthquakes
- Stress accumulated by long-term creep on the ATF can be released by failure of hanging wall splay faults

Supporting Information:
- Supporting Information S1
- Data Set S1
- Data Set S2

Correspondence to:
L. Anderlini,
letizia.anderlini@ingv.it

Citation:
Anderlini, L., E. Serpelloni, and M. E. Belardinelli (2016), Creep and locking of a low-angle normal fault: Insights from the Altotiberina fault in the Northern Apennines (Italy), *Geophys. Res. Lett.*, *43*, 4321–4329, doi:10.1002/2016GL068604.

Received 9 MAR 2016
Accepted 19 APR 2016
Accepted article online 20 APR 2016
Published online 7 MAY 2016

Creep and locking of a low-angle normal fault: Insights from the Altotiberina fault in the Northern Apennines (Italy)

L. Anderlini[1], E. Serpelloni[1], and M. E. Belardinelli[2]

[1]Istituto Nazionale di Geofisica e Vulcanologia, Centro Nazionale Terremoti, Bologna, Italy, [2]Dipartimento di Fisica e Astronomia, Settore di Geofisica, Università di Bologna, Bologna, Italy

Abstract While low-angle normal faults have been recognized worldwide from geological studies, whether these structures are active or capable of generating big earthquakes is still debated. We provide new constraints on the role and modes of the Altotiberina fault (ATF) in accommodating extension in the Northern Apennines. We model GPS velocities to study block kinematics, faults slip rates and interseismic coupling of the ATF, which is active and accounts, with its antithetic fault, for a large part of the observed chain normal 3 mm/yr tectonic extension. A wide portion of the ATF creeps at the long-term slip rate (1.7 ± 0.3 mm/yr), but the shallow locked portions are compatible with $M > 6.5$ earthquakes. We suggest that positive stress accumulation due to ATF creep is most likely released by more favorable oriented splay faults, whose rupture may propagate downdip along low-angle normal fault surface and reduce the probability of occurrence of a seismic rupture of the shallower locked portion.

1. Introduction

Low-angle normal faults (LANFs), very low dipping (0–30°) faults, or extensional detachments, have been extensively mapped in areas of continental extension. These structures have been first recognized from geological studies and imaged by seismic reflection data in the Basin and Range province, U.S., [e.g., *Wernicke*, 1981] and then documented in various tectonic settings affected by crustal extension [*Collettini*, 2011] (https://github.com/cossatot/LANF_gis).

Geological evidence suggests that LANFs played a major role in accommodating crustal extension, with fault rocks characterized by brittle-frictional characters formed in the upper seismogenic crust [e.g., *Collettini and Holdsworth*, 2004; *Jolivet et al.*, 2010; *Hayman et al.*, 2003]. Despite these widespread evidences, they remain enigmatic tectonic structures. In particular, it is not clear if LANFs are capable of generating earthquakes. This stands because brittle failure on LANFs is in conflict with Andersonian theory of faulting, as typically applied to the upper crust [*Axen*, 2004] and because observations of seismic faulting on LANFs are sparse and ambiguous [e.g., *Wernicke*, 1995]. As detachments structures, they are also considered as anomalously weak (static friction coefficient $\mu_s \ll 0.6$) and seats of aseismic slip [e.g., *Collettini and Holdsworth*, 2004; *Collettini*, 2011].

Evidence for active low-angle normal faulting is documented in numerous field-based structural studies [e.g., *Hayman et al.*, 2003; *Collettini and Holdsworth*, 2004] and interpretation of seismic reflection profiles [*Roy and Kenneth*, 1992; *Barchi et al.*, 1998; *Laigle et al.*, 2000]. Other evidence for currently active LANFs is based on microseismicity studies [*Rigo et al.*, 1996; *Chiaraluce et al.*, 2007]. On the contrary, geodetic evidence of low-angle normal faulting is more limited [e.g., *Hreinsdóttir and Bennett*, 2009], and definite inference of the spatial distribution of interseismic coupling is not yet reported in the literature.

In this work we use a dense network of Global Positioning System (GPS) stations to study crustal deformation and fault kinematics of the Umbria-Marche sector of the Northern Apennines of Italy (Figure 1). Here an active LANF, the Altotiberina fault (ATF) [*Barchi et al.*, 1998; *Boncio et al.*, 2000], is imaged by seismological and geodetic observations [*Chiaraluce et al.*, 2007; *Hreinsdóttir and Bennett*, 2009] and a multidisciplinary near fault research infrastructure [TABOO, *Chiaraluce et al.*, 2014] is operating as a part of the European Plate Observing System (https://www.epos-ip.org) Near Fault Observatories infrastructures. Balanced restored geological cross sections show that the ATF represents a major fault accommodating up to 10 km of regional extension since 3 Ma [*Barchi et al.*, 1998]. However, the role of the east dipping ATF in the present-day SW-NE extension is still not clear. This sector of the Apennines is characterized by high geodetic deformation

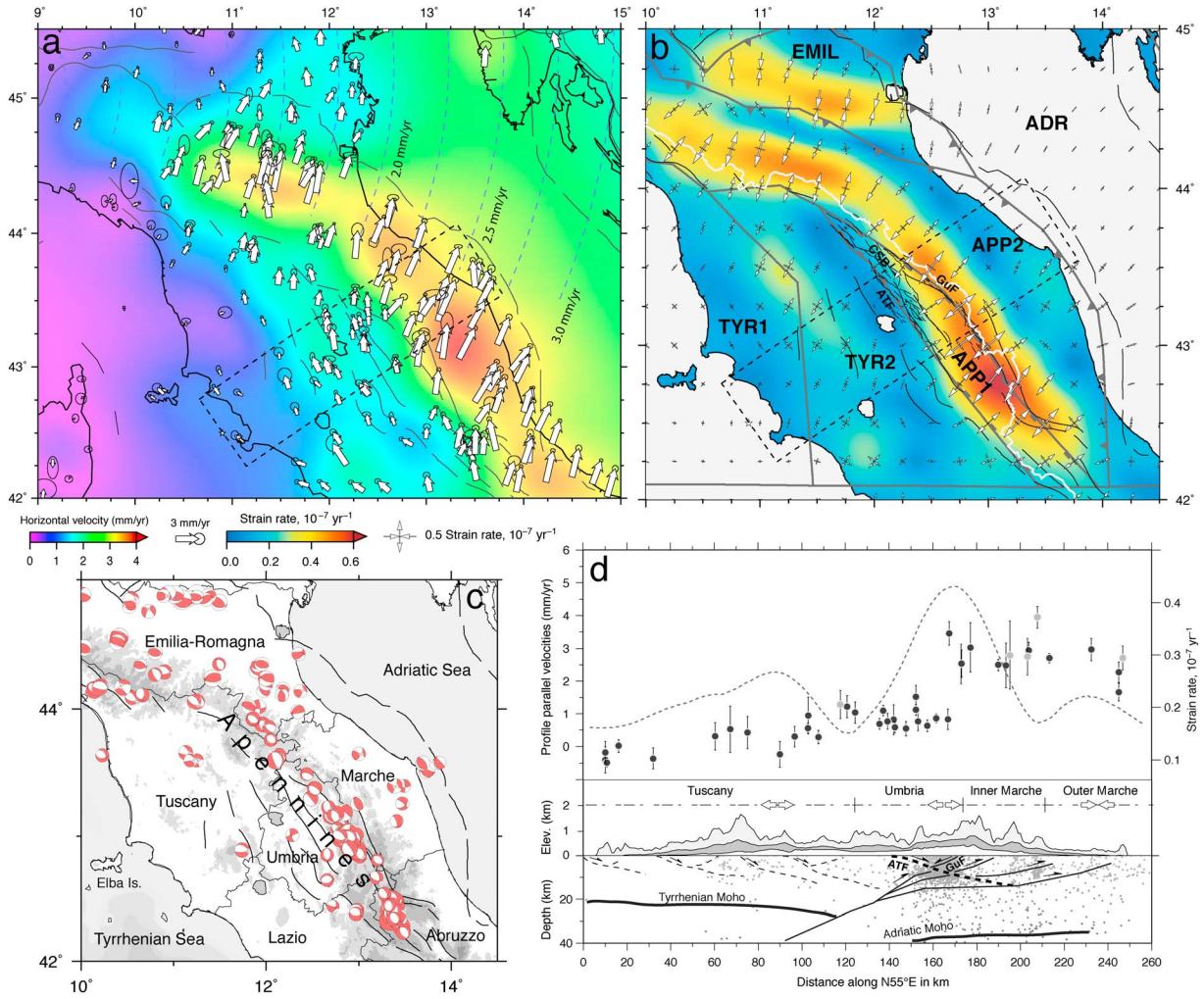

Figure 1. Seismotectonics and crustal deformation field. (a) GPS horizontal velocities (with 95% error ellipses), in a fixed-Eurasian frame, superimposed on a map of the continuous multiscale velocity field. The dashed blue lines indicate the small circles around the geodetic pole of rotation showing the motion direction of Adria relative to Eurasia (Table S1); the black lines show major faults (http://ccgm.free.fr). (b) Principal strain rate axes superimposed on a map of the total (scalar) strain rate field; labels indicate the blocks used in the kinematic modeling (section 4) and the bold gray lines indicate the blocks boundaries; the white lines show the regional drainage divide; the Gubbio fault (GuF) and the Città di Castello-San Sepolcro basin (CSB) are indicated. (c) Geographical context and focal mechanisms (http://www.bo.ingv.it/RCMT). (d) Cross section along the dashed box in Figures 1a and 1b. (top) Profile-parallel velocity components (circles with 1σ error bars, with the gray circles indicating survey-mode stations) and scalar strain rate (dashed line). (bottom) Topography and cross section view of the subsurface structures (following *Chiaraluce et al.* [2007]). White arrows indicate the known tectonic regimes (compressional or extensional) of the different geographic provinces. Instrumental seismicity (gray dots) is taken from http://iside.rm.ingv.it.

rates [*D'Agostino et al.*, 2009; *Bennett et al.*, 2012], but no large earthquake has been attributed to the ATF [*Rovida et al.*, 2011]. On the contrary, major historical earthquakes are attributed to faulting on west dipping normal faults that cut the ATF hanging wall [*Boncio et al.*, 2004; *Chiaraluce et al.*, 2004] (Figure 1d). Several lines of evidence, including fine grained foliations composed of velocity strengthening phyllosilicate-minerals documented along ancient and exhumed LANF of the Apenninic chain [*Collettini and Holdsworth*, 2004], high-fault fluid overpressures observed in footwall boreholes (~85% lithostatic pressure at 3.7–4.8 km depth), persistent microseismicity [*Chiaraluce et al.*, 2007] located in the ATF hanging wall (see Figure 2a), and the pattern of geodetic deformation [*Hreinsdóttir and Bennett*, 2009] suggest that the ATF may slip primarily by aseismic creep below ~4 km depth in the crust. However, the spatial distribution of creep on the ATF plane is not known; thus, its seismogenic potential is still debated.

We use an elastic block model approach [e.g., *McCaffrey*, 2002] to retrieve crustal blocks rotations and geodetic slip rates. We parameterize the subsurface geometry of the ATF using high-resolution constraints from

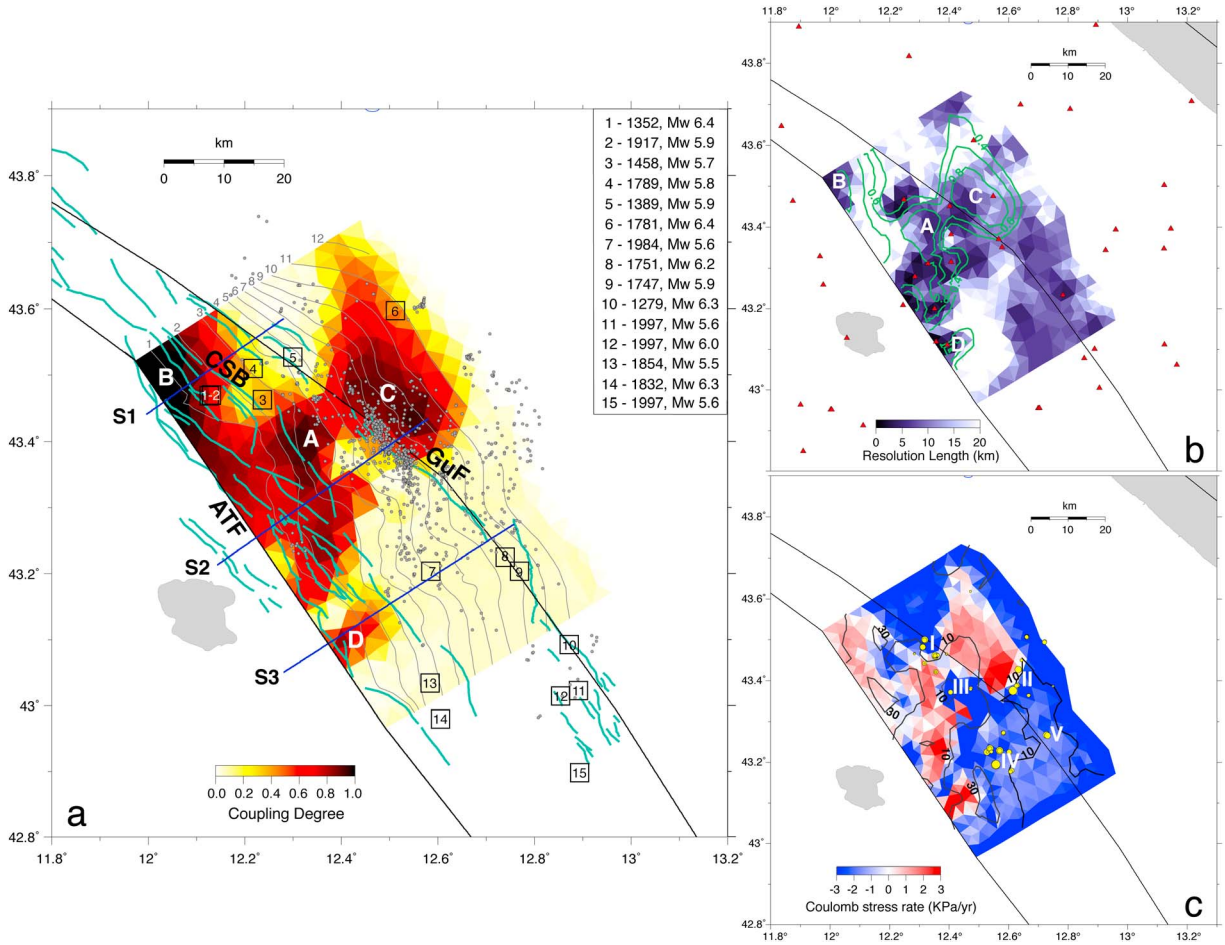

Figure 2. (a) Distribution of IC on the ATF (asperities are labeled by capitol letters), with relocated microseismicity (gray dots) and historical seismicity (numbered open squares); the thin gray lines show isodepths (km) of the ATF surface (from *Mirabella et al.* [2011]); the green lines show the traces of antithetic and synthetic faults; the blue lines (S1–S3) refer to Figure 3. (b) Resolution length (RL, in km) with contouring of the IC values (green lines), asperity labels, and GPS stations positions (red triangles). (c) Coulomb stressing rate distribution on the ATF surface with contouring of the RL (black lines) and location of repeating earthquakes (yellow circles, after *Chiaraluce et al.* [2007]), grouped in different clusters (indicated by roman numbers).

seismic reflection data and seismicity, estimating the spatial distribution of interseismic fault coupling or creep and discussing the results in terms of LANF kinematics, seismic potential, and fault mechanics.

2. Tectonic Setting

The Umbria-Marche Apennines are an arc-shaped, NE verging, thrust and fold belt, corresponding to the easternmost sector of the Northern Apennines (Figure 1). This area is characterized by the presence of a complex pattern of thrusts, folds, and normal faults, reflecting the superposition of two tectonic phases: an upper Miocene-lower Pleistocene compressional phase, which formed the N-NE verging thrusts and folds, and a Quaternary extensional phase, which formed the intermountain basins bounded by NW-SE trending normal faults, offsetting the earlier fabrics. The interpretation of the CROP03 seismic reflection profiles [*Pialli et al.*, 1998] shows that a significant amount of extension within the brittle upper crust has been accommodated by several east dipping LANFs with associated antithetic and synthetic faults. Older parts of the extensional system are exhumed to the west, in the Tyrrhenian islands (e.g., Elba, Figure 1c) and Tuscany [*Collettini and Holdsworth*, 2004], while the ATF, which is the easternmost one, is located in the inner sector of the Umbria-Marche Apennines (Figure 1d). This sector is presently extending at rates of 2–3 mm/yr, as documented by geodetic data [*Serpelloni et al.*, 2006; *D'Agostino et al.*, 2009; *Bennett et al.*, 2012], in agreement with seismotectonic observations [*Pondrelli et al.*, 2006] (Figure 1c). The area of maximum extension

is concentrated across a 30–40 km wide zone coinciding with the area of the strongest seismic moment release [*D'Agostino et al*., 2009]. In the past 30 years, two main seismic sequences occurred in this area (Figure 2a): the 1984 Gubbio sequence (M_w 5.6) and the 1997 Colfiorito sequence (M_w 6.0, 5.7, and 5.6), that are both related to SW dipping normal faults.

3. GPS Data, Strain Rates, and Kinematics

The GPS velocity field shown in Figure 1a has been obtained analyzing data from several continuous GPS (cGPS) networks operating in the study area, integrated by survey-mode (sGPS) data collected during the Retreating-Trench, Extension, and Accretion Tectonics, RETREAT, project [*Bennett et al*., 2012], following a three-step approach (as in *Serpelloni et al*. [2013]), which is detailed in the supporting information. Figure 1 a shows horizontal velocities in a fixed-Eurasian reference frame obtained by minimizing the velocities of a set of cGPS sites located in the stable part of central Europe (see Table S1 and Data Set S2). Velocity estimates in the IGb08 reference frame and related uncertainties are reported in Data Set S1.

Figure 1a shows a continuous map of the ground speed obtained using a spherical wavelet-based approach [*Tape et al*., 2009] (see supporting information for additional information). The SW-NE oriented velocity gradient, with northeastward velocities increasing toward the Adriatic Sea corresponds with a clockwise rotation of the velocity directions. The Adriatic side of this sector of the Apennines (east of longitude 12.5°E) moves coherently but faster (on average up to 0.5 to 1 mm/yr faster) than predicted by the geodetic Adria-Eurasia relative rotation pole (see Figure 1a and Table S1 in the supporting information). These faster velocities imply shortening near and offshore the Adriatic coast, in agreement with focal mechanisms, which can be ascribed to geodynamic processes associated to the Adriatic slab [*Bennett et al*., 2012; *Barba et al*., 2008].

All these features well map into the horizontal strain rate field, shown in Figure 1b, where a scalar value of the strain rate tensor is estimated as the square root of the sum of squares of all its components $|\dot{\epsilon}| = \sqrt{\dot{\varepsilon}_x^2 + \dot{\varepsilon}_{xy}^2 + \dot{\varepsilon}_{yx}^2 + \dot{\varepsilon}_{yy}^2}$ [see *Tape et al*., 2009]. The highest strain rate values (~0.67×10^{-7} year^{-1} of NE-SW oriented extension) are located along the regional drainage divide. NE-SW oriented shortening is high (up to 0.5×10^{-7} year^{-1}) at the foothills of the Northern Apennines front (the Emilia Po Plain) and continues to the SE in the Adriatic offshore, at lower rates. SW-NE oriented shortening is present in the Marche region, approaching the Adriatic coast, and a transition between the two strain regimes occurs about at longitude 13°E. A belt of relatively higher strain rates (0.3–0.4×10^{-7} year^{-1}), with ~ NE-SW oriented extension, is present in the Tyrrhenian sector (Tuscany) of the study area.

Figure 1d shows that the sector of the Northern Apennines enclosed by the dashed box in Figure 1 is extending at a rate of ~3 mm/yr from the Tyrrhenian to the Adriatic coast. About 1 mm/yr of the SW-NE extension is taken up in the Tuscany portion, where limited crustal seismicity is recorded. The Umbria-Marche boundary shows a sharp jump in the profile-parallel velocities, with ~2 mm/yr of extension occurring within few kilometers. This region is characterized by seismicity that is mostly confined in the ATF hanging wall. To the northeast, crustal earthquakes are localized at the boundary between the inner and outer Marche Apennines and, less in number, near and offshore the Adriatic coast.

4. Modeling

4.1. Kinematic Model

In order to investigate the role of the ATF and other faults in accommodating the measured crustal extension we use the block-modeling implementation of *Meade and Loveless* [2009], inverting geodetic velocities to estimate blocks rotation poles and block-bounding slip rates. In the modeling, GPS velocity uncertainties have been rescaled by a factor of 2.4, corresponding to the normalized RMS from the least squares estimate of the Eurasian plate rotation pole (see the supporting information for additional details).

We use seismotectonics, geodetic and geological/geophysical information, and maps of active faults [*Database of Individual Seismogenic Sources Working Group*, 2015, and reference therein] in order to develop the blocks configuration defining dips and locking depths of the block-bounding faults. We realize a wider model in order to describe the overall motion of the Tyrrhenian and Adriatic domains and test different configurations of blocks and block-bounding faults. The different model geometries and the results of an *F* ratio test for additional plate

boundaries [*Stein and Gordon*, 1984] are reported in the supporting information. The best model is reported in Figure 1b and includes two Tyrrhenian blocks, one comprising the Tyrrhenian Sea and western Tuscany (TYR1) and one (TYR2) part of the Tuscany and Umbria regions, an intermediate Apenninic block (APP1), bounded by the ATF and GuF systems, and an external Apenninic block (APP2), comprising the inner and outer Marche Apennines, easterly bounded by the Adriatic microplate thrust faults. This model provides geodetic slip rates for the Altotiberina and Gubbio faults of 1.7 ± 0.3 mm/yr (hereinafter called V_0) and of 1.5 ± 0.3 mm/yr, respectively, which are close to geologically estimated values of ~1 mm/yr for the ATF [*Collettini*, 2002] and 1.65–1.9 mm/yr for the GuF [*Collettini et al*., 2003]. A model where only the ATF accommodates extension in the Umbria-Marche Apennines (Model A in Figure S2) provides higher residuals (Table S1) and a slip rate of 2.6 mm/yr for the ATF, which is close to *Hreinsdóttir and Bennett* [2009] results, who modeled the velocity field with a single east dipping dislocation, but much higher than geological estimates (~1 mm/yr) [*Collettini*, 2002].

A subdivision of the Tyrrhenian-Tuscany domain of the study area into two blocks (TYR1 and TYR2 in Figure 1b), with a boundary located along the belt of relatively higher geodetic strain rates, is justified by our data. Our results suggest that this portion of Tuscany accommodates part of the total SW-NE extension of this sector of the Apennines, but the active faults and their seismogenic potential remain unresolved.

4.2. Interseismic Coupling

We develop a model that includes variable, nonuniform, interseismic back slip on the ATF, with the goal of studying its spatial distribution. We refine the subsurface geometry of the ATF by exploiting the high-resolution information provided by seismological, geological, and geophysical data [*Chiaraluce et al*., 2007; *Mirabella et al*., 2011]. We discretize the ATF surface into triangular dislocation elements (TDEs) (Figure S3), and we use a constrained linear least squares inversion scheme, bounding the ATF back slip equal or lower than V_0, applying a regularization by means of a Laplacian operator (see supporting information for details).

With respect to the uniform slip rate model, the heterogeneous one provides a 30% reduction of the residuals (χ^2 value) at the GPS sites that are closest to the fault surface (see Figure S5 for details on how these sites are selected). We estimate the interseismic coupling (IC, Figure 2a) defined as the back slip value to V_0 ratio for each TDE, ranging between 0 and 1, where 0 means fully uncoupled fault patches (i.e., aseismic creep) and 1 means fully coupled fault patches (i.e., elastic asperities). Figure 2a shows the coupling results, highlighting two main shallow asperities (A and B), which suggest that the fault is mainly locked down to 4–5 km depth. Another asperity, C, is located within the 7–10 km depth interval. A smaller locked area, D, limited to the first 2 km depth, is located southward, close to the fault trace.

We evaluate how much of the inverted coupling distribution is resolved by data estimating the resolution length (RL; Figure 2b), that is, the characteristic size of the smallest inhomogeneity of coupling that can be detected by the geodetic data [*Ader et al*., 2012]. To consider as resolved a coupling spatial feature, the RL should be constant on it and smaller than the feature size itself. In general, the surface elastic signal caused by a TDE located at shallow depths has a very short wavelength (few km) and can be potentially resolved only by a dense GPS network. A longer wavelength, detectable also by sparser networks, characterizes the signal associated to a deeper TDE. Figure 2b shows that on the ATF surface RL can be as good as 2 km at shallow depths, and particularly near the center of the fault model, i.e., below the denser portion of the geodetic network. RL values greater than 15 km characterize some shallow fault portions, over which GPS data are absent, and the northern part of the fault.

5. Discussion

5.1. IC Resolution and Seismic Potential

Figure 2b shows that asperities A and B, shallow and contiguous, are well resolved where we have good GPS stations coverage, suggesting that the ATF is mainly locked down to 4–5 km of depth. Instead asperity D is constrained only by two GPS sites, located just over it, and the rapid rising of RL downdip could hide the presence of a larger locked portion that is not "visible" by the GPS network. The deeper asperity C is characterized by a variable RL, that is, on average, comparable to its size, suggesting that the spatial extension of this feature might be not well constrained by data. The creeping portion in the SE sector of the ATF appears resolved by the GPS network, being its size greater than the RL. Overall, Figure 2 shows that the creeping

portions correlate with the microseismicity location (Figure 2a), including repeating earthquakes (i.e., doublets as in *Chiaraluce et al.* [2007]) on the ATF plane (Figure 2c), which can be attributed to aseismic stable-sliding behavior [e.g., *Sammis and Rice*, 2001].

Using the *Hanks and Kanamori* [1979] relationship, we estimate the equivalent moment magnitude (M_w) accumulating at the locked portions in 10^3 years. In particular we evaluate the seismic moment ($M_0 = \mu$As, with $\mu = 30$GPa) for each TDE having an IC value above a certain threshold (c_t). By varying c_t (as in *Loveless and Meade* [2015]) we identify different scenarios (as shown in Figure S6).

Considering $c_t = 0.3$ we identify one big asperity that may cause a $M_w = 6.9$ earthquake. However, no historical earthquake of this size is known [*Rovida et al.*, 2011] from 1000 A.D. If $c_t = 0.7$, two distinct asperities (A + B and C in Figures 2a and S6) able to generate $M_w = 6.7$ and $M_w = 6.5$ earthquakes, respectively, are identified. The second one seems compatible with the 1781 (M_w 6.4) earthquake (N. 6 in Figure 2a), an earthquake associated by *Brozzetti et al.* [2009] to a deep portion of the ATF, although alternative hypotheses have been proposed [e.g., *Lavecchia et al.*, 2002]. Moreover, several historical earthquakes occurred in the Città di Castello-San Sepolcro basin (CSB, N. 1–5 in Figure 2a) close to the shallow locked fault portion (A + B).

These earthquakes, among which the 1352 (M_w 6.4) is the largest one, have been attributed or to partial ruptures of the ATF, extending up-dip along its synthetic faults, or to shallow, SW dipping, antithetic faults [*Brozzetti et al.*, 2009]. This hypothesis may provide an indication on how LANFs may accommodate active tectonic extension.

5.2. Stress Rate Analysis Due to the ATF Creep

In order to investigate stress-loading effects on the ATF surface and on the hanging wall faults, due to the creeping distribution, and evaluate any relation with the distribution of microseismicity (Figure 2a), we calculate the Coulomb stressing rate, CSR, [e.g., *Stein et al.*, 1997], using the *Nikkhoo and Walter* [2015] code for TDEs (see supporting information for details). Figure 2c shows the CSR computed at the centroid of each TDE of the ATF, assuming as receiver fault mechanism the one associated to each TDE. The CSR distribution leads to an average positive CSR of 2 KPa/yr, and, as expected, positive CSR values correlate with areas of high IC (i.e., locked portions of the fault). Such a stressing rate is slightly higher than the upper bound of the interval reported by *Catalli et al.* [2008] for this sector of the Apennines. In order to have a seismic event, the cumulative reloaded stress should be comparable to the stress drop of the last earthquake (for a constant static friction). Assuming a typical stress drop of 5 MPa for a $M_w = 6.5$ earthquake [*Causse et al.*, 2014], a 2 KPa/yr stressing rate would reload such a stress drop in ~2500 years. This time interval is much longer than the completeness time interval for $M_s \geq 6$ events in the historical seismic catalogue, which is shorter than 700 years for the study area [*Albarello et al.*, 2001].

Figure 2c shows that most of repeating earthquakes (REs) on the ATF are located close to patches characterized by positive stressing rates (groups I–III), providing a validation of our IC model, following *Sammis and Rice* [2001]. On the contrary, other REs occur in shadow zones (groups IV and V) for which we have two possible explanations: (a) these events may be produced by the failure of tiny fault patches, surrounded by wider creeping fault portions that continuously may load them [*Rubin et al.*, 1999; *Collettini et al.*, 2011] and (b) these events (mainly group IV) occur close to a locked portion of ATF that is not detected by our solution, as discussed in section 5.1.

We compute the CSR in the ATF surrounding medium considering different receiving faults identified in the ATF hanging wall. Figure 3 shows three cross sections of stressing rate values computed for the main antithetic (first column) and synthetic faults (second column). Positive stressing rates affect most of them, mainly for those located in the CSB (profile S1 of Figure 3). The persistent microseismicity occurring in the ATF hanging wall (Figure 2a) highlights also an antithetic, 60° southwestward dipping, normal fault system [*Chiaraluce et al.*, 2007] for which we evaluate the expected CSR due to ATF creep at different depths (Fig. S7). Our results show that most of these off-fault events fall in shadowed zones (negative values of CSR), suggesting that further processes should be considered in order to explain them.

The positive stress buildup found on most of the synthetic and antithetic ATF faults may suggest a mechanism by which LANF can accommodate the tectonic extension. Having a larger dip, synthetic, and antithetic faults located in the hanging wall of a LANF are more likely to slip in an Andersonian sense. Stress analyses

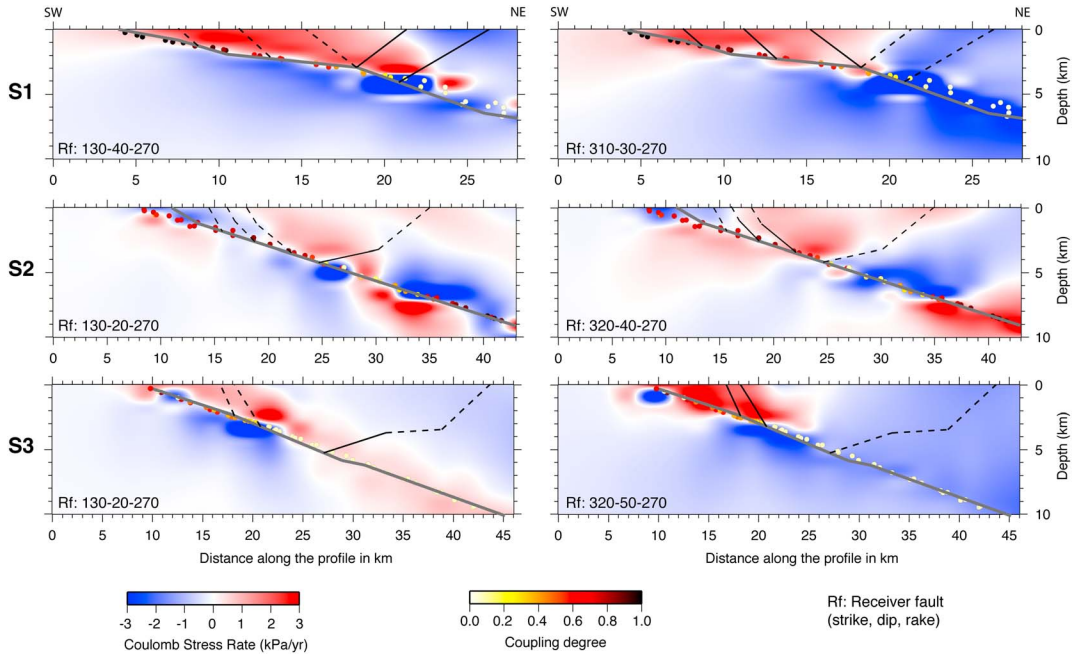

Figure 3. Cross sections through the ATF showing the Coulomb stressing rates generated by the ATF creep rate distribution assuming as receiver faults both antithetic and synthetic faults located in the ATF hanging wall. The traces of the cross sections S1–S3 are shown in Figure 2a. The geometry of synthetic and antithetic receiver faults are taken from published geological cross sections. In particular, for S1 we use faults derived from *Brozzetti et al*. [2009] and for S2 and S3 we use faults derived from *Mirabella et al*. [2011]. In each cross section, the bold gray line shows the ATF, and the colored circles show the IC values at the TDEs intersecting the cross section; the black lines show the synthetic and antithetic faults. Each panel reports the CSR estimates for a specific receiver fault (Rf) geometry indicated by its strike, dip, and rake angles, reported in the lower left corner. Active (receiving) faults are shown in each panel by the solid black lines, whereas the dashed lines indicate other faults in the ATF hanging wall.

[*Axen*, 1999; *Scholz*, 2011] and mechanical models [*Bruhn and Schultz*, 1996] show that splay faults should be simultaneously active with the low-angle master fault, being potential sites of seismic nucleation, which may extend downdip along the low-angle master fault. The present study shows that creep on ATF may encourage seismic failure on synthetic and antithetic faults. This seismogenic scenario is someway compatible to the one proposed by *Brozzetti et al*. [2009]. In turn, on one hand failure on splay faults may trigger seismic failure [*Axen*, 1999] or transient acceleration of creep on locked or unlocked portions, respectively, located downdip along the ATF fault; on the other hand it may decrease the Coulomb failure stress on the ATF locked up-dip portions (Figure S8). This last effect may allow for a release of the shallow positive stress buildup due to ATF creeping portions, reducing there the probability of occurrence of a seismic event.

6. Conclusions

Using a dense network of GPS stations and a block-modeling approach, we study crustal deformation rates and fault slip rates in the Northern Apennines, which are extending at 3 mm/yr and where a low-angle normal fault is active. Our preferred model implies that ~1 mm/yr of the estimated SW-NE extension is accommodated in the inner (Tyrrhenian) sector of the study area and ~2 mm/yr are accommodated by activity of the low-angle northeastward dipping Altotiberina fault and its antithetic fault system. The high density of GPS stations allows us to provide the first image of spatially variable interseismic coupling on a LANF. We find that the ATF is mainly locked down to a depth of 4–5 km, being the largest part of the fault surface creeping at the long-term geodetic slip rate (1.7 ± 0.3 mm/yr), except for a deeper asperity located between 7 and 10 km of depth. The main creeping portion correlates with relocated microseismicity and in particular with the location of repeating earthquakes. The locked portions of the ATF corresponds to potential M_w 6.7 and M_w 6.5 earthquakes over a time interval of 10^3 years, but such large events are not present in the historical seismic catalog for this area. The analysis of the stress rate field induced by the creep rate distribution on both the

ATF surface and on its surrounding media shows positive stress build up on the locked ATF asperities and on most of the normal splay faults in the ATF hanging wall. These splay faults may release the positive stress buildup on shallow locked portions of ATF, favoring potential seismic slip or transient acceleration of creep on deeper fault portions, suggesting that actually this LANF may have experienced both seismic ruptures and historical splay faults events.

Acknowledgments
We thank the Editor, Andrew Newman, Cristiano Collettini, and an anonymous reviewer for their detailed and constructive comments that have greatly improved this paper. L.A. has been supported by Progetto "PREMIALE 2011: Studio multidisciplinare della fase di preparazione di un terremoto." We thank John P. Loveless and Brendan J. Meade for their help in the use of the block-modeling code, and Carl Tape for making available his multiscale strain rate estimation code. We thank Romano Camassi, Lauro Chiaraluce, Luisa Valoroso, Francesco Mirabella, and Luigi Vadacca for their helpful comments and discussions. Some of the figures have been created using the Generic Mapping Tools (GMT) software [*Wessel and Smith*, 1998]. All the data presented in this work are made available in the supporting information.

References

Ader, T., et al. (2012), Convergence rate across the Nepal Himalaya and interseismic coupling on the Main Himalayan Thrust: Implications for seismic hazard, *J. Geophys. Res.*, *117*, B04403, doi:10.1029/2011JB009071.

Albarello, D., R. Camassi, and A. Rebez (2001), Detection of space and time heterogeneity in the completeness of a seismic catalog by a statistical approach: An application to the Italian area, *Bull. Seismol. Soc. Am.*, *91*(6), 1694–1703, doi:10.1785/0120000058.

Axen, G. J. (1999), Low-angle normal fault earthquakes and triggering, *Geophys. Res. Lett.*, *26*, 3693–3696, doi:10.1029/1999GL005405.

Axen, G. J. (2004), Mechanics of low-angle normal faults, in *Rheology and Deformation of the Lithosphere at Continental Margins*, *MARGINS Theor. and Exp. Earth Sci. Ser.*, edited by G. D. Karner et al., pp. 46–91, Columbia Univ. Press, New York.

Barba, S., M. M. C. Carafa, and E. Boschi (2008), Experimental evidence for mantle drag in the Mediterranean, *Geophys. Res. Lett.*, *35*, L06302, doi:10.1029/2008GL033281.

Barchi, M., R. Minelli, and G. Pialli (1998), The CROP 03 profile: A synthesis of results on deep structures of the Northern Apennines, *Mem. Soc. Geol. Ital.*, *52*, 383–400.

Bennett, R. A., et al. (2012), Syn-convergent extension observed using the RETREAT GPS network, Northern Apennines, Italy, *J. Geophys. Res.*, *117*, B04408, doi:10.1029/2011JB008744.

Boncio, P., F. Brozzetti, and G. Lavecchia (2000), Architecture and seismotectonics of a regional low-angle normal fault zone in central Italy, *Tectonics*, *19*, 1038–1055, doi:10.1029/2000TC900023.

Boncio, P., G. Lavecchia, and B. Pace (2004), Defining a model of 3D seismogenic sources for Seismic Hazard Assessment applications: The case of central Apennines (Italy), *J. Seismol.*, *8*, 407–425, doi:10.1023/B:JOSE.0000038449.78801.05.

Brozzetti, F., P. Boncio, G. Lavecchia, and B. Pace (2009), Present activity and seismogenic potential of a low-angle normal fault system (Città di Castello, Italy): Constraints from surface geology, seismic reflection data and seismicity, *Tectonophysics*, *463*, 31–46, doi:10.1016/j.tecto.2008.09.023.

Bruhn, R. L., and R. A. Schultz (1996), Geometry and slip distribution in normal fault systems: Implications for mechanics and fault-related hazards, *J. Geophys. Res.*, *101*, 3401–3412, doi:10.1029/95JB03253.

Catalli, F., M. Cocco, R. Console, and L. Chiaraluce (2008), Modeling seismicity rate changes during the 1997 Umbria-Marche sequence (central Italy) through a rate- and state-dependent model, *J. Geophys. Res.*, *113*, B11301, doi:10.1029/2007JB005356.

Causse, M., L. A. Dalguer, and P. M. Mai (2014), Variability of dynamic source parameters inferred from kinematic models of past earthquakes, *Geophys. J. Int.*, *196*(3), 1754–1769, doi:10.1093/gji/ggt478.

Chiaraluce, L., et al. (2004), Complex normal faulting in the Apennines thrust-and-fold belt: The 1997 seismic sequence in central Italy, *Bull. Seismol. Soc. Am.*, *94*(1), 99–116, doi:10.1785/0120020052.

Chiaraluce, L., C. Chiarabba, C. Collettini, D. Piccinini, and M. Cocco (2007), Architecture and mechanics of an active low-angle normal fault: Alto Tiberina Fault, Northern Apennines, Italy, *J. Geophys. Res.*, *112*, B10310, doi:10.1029/2007JB005015.

Chiaraluce, L., et al. (2014), The Alto Tiberina Near Fault Observatory (Northern Apennines, Italy), *Ann. Geophys.*, *57*(3), S0327, doi:10.4401/ag-6426.

Collettini, C. (2002), Hypothesis for the mechanics and seismic behaviour of low-angle normal faults: The example of the Altotiberina fault Northern Apennines, *Ann. Geophys.*, *45*(5), 683–698, doi:10.4401/ag-3531.

Collettini, C. (2011), The mechanical paradox of low-angle normal faults: Current understanding and open questions, *Tectonophysics*, *510*, 253–268, doi:10.1016/j.tecto.2011.07.015.

Collettini, C., and R. E. Holdsworth (2004), Fault zone weakening processes along low-angle normal faults: Insights from the Zuccale Fault, Isle of Elba, Italy, *J. Geol. Soc.*, *161*, 1039–1051, doi:10.1144/0016-764903-179.

Collettini, C., L. Chiaraluce, F. Mirabella, S. Pucci, and M. R. Barchi (2003), The Gubbio seismogenic normal fault: Can different methods picture the same object?, *J. Geodyn.*, *36*, 51–66, doi:10.1016/S0264-3707(03)00038-3.

Collettini, C., A. Niemeijer, C. Viti, S. A. F. Smith, and C. Marone (2011), Fault structure, frictional properties and mixed-mode fault slip behavior, *Earth Planet. Sci. Lett.*, *311*(3–4), 316–327, doi:10.1016/j.epsl.2011.09.020.

D'Agostino, N., S. Mantenuto, E. D'Anastasio, A. Avallone, M. Barchi, C. Collettini, F. Radicioni, A. Stoppini, and G. Fastellini (2009), Contemporary crustal extension in the Umbria–Marche Apennines from regional CGPS networks and comparison between geodetic and seismic deformation, *Tectonophysics*, *476*(1-2), 3–12, doi:10.1016/j.tecto.2008.09.033.

Database of Individual Seismogenic Sources Working Group (2015), Database of Individual Seismogenic Sources (DISS), Version 3.2.0: A compilation of potential sources for earthquakes larger than M 5.5 in Italy and surrounding areas, Ist. Naz. di Geofis. e Vulcanol. (INGV), doi:10.6092/INGV.IT-DISS3.2.0. [Available at http://diss.rm.ingv.it/diss/.]

Hanks, T. C., and H. Kanamori (1979), A moment magnitude scale, *J. Geophys. Res.*, *84*, 2348–2350, doi:10.1029/JB084iB05p02348.

Hayman, N. W., J. R. Knott, D. S. Cowan, E. Nemser, and A. Sarna-Wojcicki (2003), Quaternary low-angle slip on detachment faults in Death Valley, California, *Geology*, *31*(4), 343–346, doi:10.1130/0091-7613(2003)031<0343:QLASOD>2.0.CO;2.

Hreinsdóttir, S., and R. Bennett (2009), Active aseismic creep on the Alto Tiberina low-angle normal fault, Italy, *Geology*, *37*, 683–686, doi:10.1130/G30194A.1.

Jolivet, L., E. Lecomte, B. Huet, Y. Denèle, O. Lacombe, L. Labrousse, L. Le Pourhiet, and C. Mehl (2010), The north cycladic detachment system, *Earth Planet. Sci. Lett.*, *289*, 87–104, doi:10.1016/j.epsl.2009.10.032.

Laigle, M., A. Hirn, M. Sachpazi, and N. Roussos (2000), North Aegean crustal deformation: An active fault imaged to 10 km depth by reflection seismic data, *Geology*, *28*(1), 71–74, doi:10.1130/0091-7613(2000)28<71:NACDAA>2.0.CO;2.

Lavecchia, G., P. Boncio, F. Brozzetti, M. Stucchi, and I. Leschiutta (2002), New criteria for seismotectonic zoning in Central Italy: Insights from the Umbria–Marche Apennines, *Boll. Soc. Geol. Ital.*, *121*(1), 881–891.

Loveless, J. P., and B. J. Meade (2015), Kinematic barrier constraints on the magnitudes of additional great earthquakes off the east coast of Japan, *Seismol. Res. Lett.*, *86*, 202–209, doi:10.1785/0220140083.

McCaffrey, R. (2002), Crustal block rotations and plate coupling, in *Plate Boundary Zones*, edited by S. Stein and J. T. Freymueller, pp. 101–122, AGU, Washington, D. C., doi:10.1029/GD030p0101

Meade, B. J., and J. P. Loveless (2009), Block modeling with connected fault-network geometries and a linear elastic coupling estimator in spherical coordinates, *Bull. Seismol. Soc. Am.*, *99*, 3124–3139, doi:10.1785/0120090088.

Mirabella, F., F. Brozzetti, A. Lupattelli, and M. R. Barchi (2011), Tectonic evolution of a low-angle extensional fault system from restored cross-sections in the Northern Apennines (Italy), *Tectonics*, *30*, TC6002, doi:10.1029/2011TC002890.

Nikkhoo, M., and T. R. Walter (2015), Triangular dislocation: An analytical, artefact-free solution, *Geophys. J. Int.*, *201*, 1117–1139, doi:10.1093/gji/ggv035.

Pialli, G., M. Barchi, and G. Minelli (1998), Results of the CROP03 deep seismic reflection profile, *Mem. Soc. Geol. Ital.*, *52*, 1–657.

Pondrelli, S., S. Salimbeni, G. Ekstrom, A. Morelli, P. Gasperini, and G. Vannucci (2006), The Italian CMT dataset from 1977 to the present, *Phys. Earth Planet. Inter.*, *159*, 286–303, doi:10.1016/j.pepi.2006.07.008,159/3-4.

Rigo, A., H. Lyon-Caen, R. Armijo, A. Deschamps, D. Hatzfeld, K. Makropoulos, P. Papadimitriou, and I. Kassaras (1996), A microseismic study in the western part of the Gulf of Corinth (Greece): Implications for large-scale normal faulting mechanisms, *Geophys. J. Int.*, *126*(3), 663–688, doi:10.1111/j.1365-246X.1996.tb04697.x.

Rovida, A., R. Camassi, P. Gasperini, and M. Stucchi (2011), CPTI11, the 2011 version of the Parametric Catalogue of Italian Earthquakes, Ist. Naz. di Geofis. e Vulcanol., Milano, Bologna, doi:10.6092/INGV.IT-CPTI11.

Roy, A. J., and L. L. Kenneth (1992), Seismic reflection evidence for seismogenic low-angle faulting in south-eastern Arizona, *Geology*, *20*, 597–600, doi:10.1130/0091-7613(1992)020<0597:SREFSL>2.3.CO;2.

Rubin, A. M., D. Gillard, and J.-L. Got (1999), Streaks of microearthquakes along creeping faults, *Nature*, *400*, 635–641, doi:10.1038/23196.

Sammis, C. G., and J. R. Rice (2001), Repeating earthquakes as low-stress-drop events at a border between locked and creeping fault patches, *Bull. Seismol. Soc. Am.*, *91*(3), 532–537, doi:10.1785/0120000075.

Scholz, C. H. (2011), First-order splay faults: Dip-slip examples, *Geol. Soc. London Spec. Publ.*, *359*(1), 313–318, doi:10.1144/SP359.17.

Serpelloni, E., M. Anzidei, P. Baldi, G. Casula, and A. Galvani (2006), GPS measurement of active strains across the Apennines, *Ann. Geophys.*, *49*(1), 319–329, doi:10.4401/ag-5756.

Serpelloni, E., C. Faccenna, G. Spada, D. Dong, and S. D. P. Williams (2013), Vertical GPS ground motion rates in the Euro-Mediterranean region: New evidence of velocity gradients at different spatial scales along the Nubia-Eurasia plate boundary, *J. Geophys. Res. Solid Earth*, *118*, 6003–6024, doi:10.1002/2013JB010102.

Stein, R. S., A. A. Barka, and J. H. Dieterich (1997), Progressive failure on the North Anatolian fault since 1939 by earthquake stress triggering, *Geophys. J. Int.*, *128*, 594–604, doi:10.1111/j.1365-246X.1997.tb05321.x.

Stein, S., and R. Gordon (1984), Statistical test of additional plate boundaries from plate motion inversion, *Earth Planet. Sci. Lett.*, *69*(2), 401–412, doi:10.1016/0012-821X(84)90198-5.

Tape, C., P. Musé, M. Simons, D. Dong, and F. Webb (2009), Multiscale estimation of GPS velocity fields, *Geophys. J. Int.*, *179*(2), 945–971, doi:10.1111/j.1365-246X.2009.04337.x.

Wernicke, B. (1981), Low angle normal faults in the Basin and Range Province: Nappe tectonics in an extending orogene, *Nature*, *291*, 645–648, doi:10.1038/291645a0.

Wernicke, B. (1995), Low-angle normal faults and seismicity: A review, *J. Geophys. Res.*, *100*, 20,159–20,174, doi:10.1029/95jb01911.

Wessel, P., and W. H. F. Smith (1998), New, improved version of the generic mapping tools released, *Eos Trans. AGU*, *79*(47), 579, doi:10.1029/98EO00426.